The Astrophysical Journal, 687:1070–1074, 2008 November 10

COSMIC RAY COMPACTION OF POROUS INTERSTELLAR ICES

U. Raut, M. Famá, M. J. Loeffler, and R. A. Baragiola
Laboratory of Atomic and Surface Physics, University of Virginia, Thornton Hall B-114, Charlottesville, VA 22904;
ur5n@virginia.edu, maf7e@virginia.edu, mjl8r@virginia.edu, raul@virginia.edu
Received 2008 May 20; accepted 2008 July 28

ABSTRACT

We studied the compaction of microporous vapor-deposited ice films under irradiation with different ions in the 80–400 keV energy range. We found that porosity decreases exponentially with irradiation fluence, with a mean compaction area per ion that scales linearly with the stopping power of the projectile S above a threshold $S_t = 4$ eV Å^{-1}. The experiments roughly follow a universal dependence of ion-induced compaction with restricted dose (eV molecule^{-1}). This behavior can be used to extrapolate our results to conditions of the interstellar medium. Relating our results to ionization rates of interstellar H_2, we estimate that porous ice mantles on grains in dense molecular clouds are compacted by cosmic rays in ~10–50 million years.

Subject headings: cosmic rays — ISM: molecules — methods: laboratory — radiation mechanisms: nonthermal

Online material: color figures

1. INTRODUCTION

Ice films grown from condensation of water vapor onto cold surfaces in the laboratory are microporous (Mayer & Pletzer 1986; Raut et al. 2007a; Stevenson et al. 1999). Similar conditions may form porous ice coatings on grains in cold molecular interstellar clouds. Identification of porosity by remote sensing can be based on weak infrared absorption features near 2.7 μm due to the O-H vibration of dangling bonds on the pore surfaces (Rowland & Devlin 1991). To date, there have been no reports of the detection of dangling bond absorptions in the infrared spectra of interstellar ices (Keane et al. 2001), suggesting that they are nonporous. Interstellar ice could have formed in a nonporous state, perhaps from chemical reactions on the surface of the dust grains, or porous ice could be compacted by transient heating or radiation. Laboratory studies suggest that, over the lifetime of the molecular clouds (~10^7 yr), the porosity of ice coatings could be reduced by cosmic rays impacts (Palumbo 2006; Raut et al. 2007b). Although the details of physical processes by which compaction occurs are not fully understood, we posited earlier that the energy deposited by the ions causes molecular motion that alters the ice structure and minimizes the internal surface energy via the removal of pores. Compaction should therefore depend on the energy deposited by the ion. In this study, we varied the type and energy of the projectiles to study the dependence of compaction on the stopping power, the energy loss per unit path length. The experimental results are compared with theoretical models that describe amorphization and damage created by fast ions in a variety of solid targets. We use these models to extrapolate our results to the interstellar medium conditions, in order to estimate compaction timescales for porous interstellar ice mantles, which are constantly bombarded with cosmic rays.

2. EXPERIMENTAL PROCEDURE

Experiments were performed in an ultrahigh vacuum chamber (base pressure ~10^{-10} Torr). Thin ice films were deposited onto the polished surface of a gold-coated quartz crystal microbalance at a rate of ~10^{15} molecules cm^{-2} s^{-1} at 30 K. Water effusing from a microcapillary array doser was incident at 45° on the surface to grow microporous ice (Raut et al. 2007b). The microbalance measures the areal mass of the films, which is converted to column density in molecules cm^{-2} by dividing by the molecular mass. Ices were irradiated at 30 K with different ions at 20° incidence. The ion beams were produced by a 30–300 kV mass-analyzed ion accelerator and rastered uniformly across the ice films. In all experiments, the column density of the ice films was small enough that the stopping power remained constant within 15% across the film thickness, as calculated using the SRIM Monte Carlo code (Ziegler & Biersack 2006). The column density of the films was chosen to be 1.58×10^{18} H_2O cm^{-2} for H and He irradiation, and 0.63×10^{18} H_2O cm^{-2} when using the less penetrating Ne and Ar ions.

Specular light reflectance spectra in the 250–800 nm wavelength range were collected at 2.5° incidence using a CCD spectrometer. The spectra showed intensity maxima and minima at different wavelengths due to the interference of light reflected from the ice-vacuum and the ice gold interfaces. We use Fresnel equations to fit the reflectance spectra and to obtain the index of refraction and the film thickness d, which together with the areal mass of the microbalance, gives the average film density ρ. The initial density of our films deposited at 45° incidence is 0.7 g cm^{-3}. This corresponds to film thickness of 0.68 and 0.27 μm for ice films irradiated with light (H, He) and heavy ions (Ne, Ar), respectively. We then derived the average film porosity, $P = 1 - \rho/\rho_c$, using $\rho_c = 0.94$ g cm^{-3} (Narten et al. 1976) for compact amorphous ice. Our films have a porosity of 0.26 ± 0.02 at growth.

3. RESULTS

Figure 1 shows the spectral reflectance of ice films before and after ion irradiation, together with fits to the Fresnel equations. The unirradiated sample has a thickness of 0.68 μm and a porosity of $P = 0.26$. Samples irradiated with 80 keV H^+ to a fluence of 10^{14} and 10^{15} ions cm^{-2} have porosities reduced to 0.14 and 0.06, respectively. The deviations between the data and the fits at low wavelengths are attributed to scattering by imperfections in the film.

Figure 2 shows the change in porosity of the ice films when irradiated with different projectiles and energies. In all cases, the porosity of the ice films dropped exponentially with irradiation fluence F from 0.26 ± 0.02 to <0.01 at a rate that depended on the ion type and energy. For instance, the fluences required to

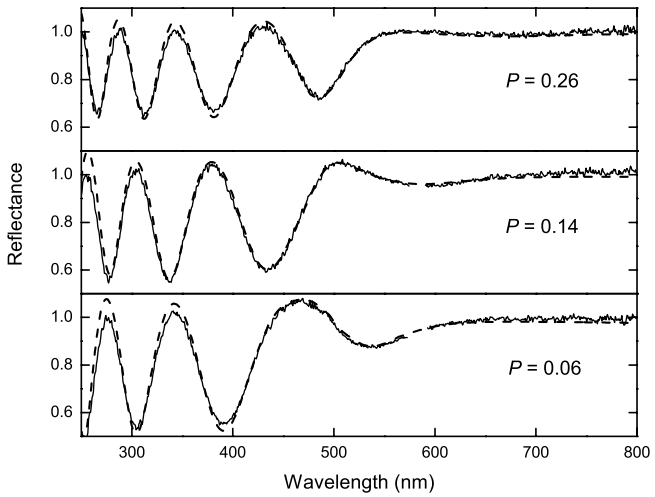

FIG. 1.—Specular reflectance spectrum of an unirradiated ice film (*top, solid line*) 0.68 μm thick with 26% porosity, together with the reflectance spectra of the film when irradiated with 80 keV H^+ to a fluence of 10^{14} ions cm^{-2} (*middle*) and 10^{15} ions cm^{-2} (*bottom*). The porosity of the film reduces to 0.14 and 0.06 from irradiation. The dashed lines are synthetic spectra generated using Fresnel's equations to match the experimental spectra. [*See the electronic edition of the Journal for a color version of this figure.*]

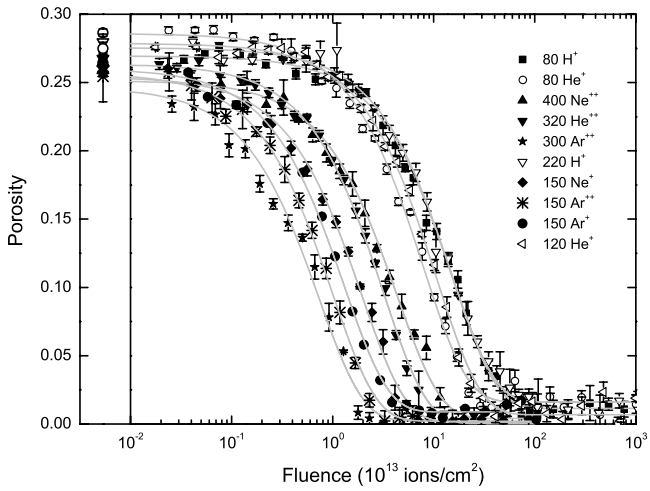

FIG. 2.—Fluence dependence of compaction for ice films deposited at 30 K at 45° incidence for different projectiles at different energies. The lines are fits to the data in the form $P(F) = P_0 \exp(-AF) + P_r$. The data points shown in the left portion of the plot are the initial porosities of the unirradiated films. [*See the electronic edition of the Journal for a color version of this figure.*]

compact ice with 80 keV protons were nearly 10 times larger than for 150 keV Ar^{++}. All the data show an exponential decay of porosity with fluence, which can be fit to the expression $P(F) = P_0 \exp(-AF) + P_r$, where P_0 is the film porosity of the unirradiated ice and P_r is a small residual porosity after irradiation. This dependence arises because a cylindrical region of area A perpendicular to the ion path is compacted by the deposited energy in proportion to the porous fraction of the film: $dP = -AFP$.

4. DISCUSSION

Several studies have shown that porous amorphous ice compacts when heated to temperature exceeding 120 K. In some of these studies the reduction in ice porosity is inferred from the decrease in gas adsorption capacity (Kimmel et al. 2001) or the decrease in the intensity of the dangling bond absorption features (Horimoto et al. 2002). At temperatures >120 K, diffusion of water molecules becomes significant, and the mobile molecules will rearrange to form compact ice, the thermodynamically favored structure. In the case of irradiation, water molecules in a small region around the path of the ion become mobile in response to the energy deposited by the ion. The radiation-enhanced diffusion allows molecules within the ion track to rearrange into a compact structure. The energy transferred from the ion to the solid is characterized by the stopping power $S = dE/dx$, given by an electronic component, S_e, due to energy transfer into electronic excitations and a nuclear component, S_n, due to elastic collisions with the target nuclei. This energy is deposited in a cylindrical region around the ion path, called the ion track. Below, we discuss briefly two theoretical models that give the radius of this track for the case of swift ions and show that they are consistent with our data.

4.1. *Fast Light Ions*

1. *Modified Lattice Potential* (*MLP*) *model*.—The MLP model (Watson & Tombrello 1985) assumes that electronic excitations created by the ion and fast secondary electrons result in a region where the transient but significant modification of the intermolecular lattice potential leads to molecular motion. This region is a cylindrical track of displaced atoms extending to a radius where the density of deposited energy is greater than a critical value ε_c. We modified the radial dependence of the energy density $\varepsilon(r)$ to a simple r^{-2} relation (Waligorski et al. 1986) outside a core region where $\varepsilon(r)$ is assumed constant, instead of the $r^{-1.73}$ in their original derivation. The radius of the core region is the lattice constant l (3.17 Å for water ice). The area of the track in this modified formalism is given by

$$A_{\rm MLP} = \frac{S_e}{\varepsilon_c\,[1 + 2\ln(R_m/l)]}, \qquad (1)$$

where R_m is the maximum transverse range of the secondary electrons, which was taken to be proportional to the square of the ion velocity (Waligorski et al. 1986). This proportionality is valid if the electrons are so fast that one can neglect the electrostatic potential of the ionized track and elastic collisions of electrons with lattice atoms.

2. *Thermal Spike model*.—The basic assumption of this model is that molecular motion in the track of the fast ions can be described as a thermal spike: a high temperature T which decays quickly with time after impact ($\sim 10^{14}$ K s^{-1}) and decreases exponentially with the square of distance from the ion path. A cylindrical volume will melt if its temperature exceeds T_m, the melting temperature of the solid. The liquid region solidifies into an amorphous structure in $\sim 10^{-11}$ s, the typical lifetime of a thermal spike (Szenes 1995), and its radius defines the size of the ion track. In this model, if the peak temperature of the thermal spike largely exceeds T_m, then the cross sectional area of the melted track is given by (Szenes 1992, 1997)

$$A_{\rm TS} = \frac{gS_e}{2.7\bar{\rho}\bar{c}T_0}, \qquad (2)$$

where g is the fraction of the electronic energy transferred into thermal motion, and $\bar{\rho}$ and $\bar{c}$ are the density and specific heat capacity of the solid averaged over the lifetime of the spike; T_0 is the difference between the melting temperature and the temperature prior to irradiation.

Whereas the thermal spike model predicts a linear dependence of A on S_e, the MLP model has an additional velocity dependence for fast ions through the maximum range of secondary electrons

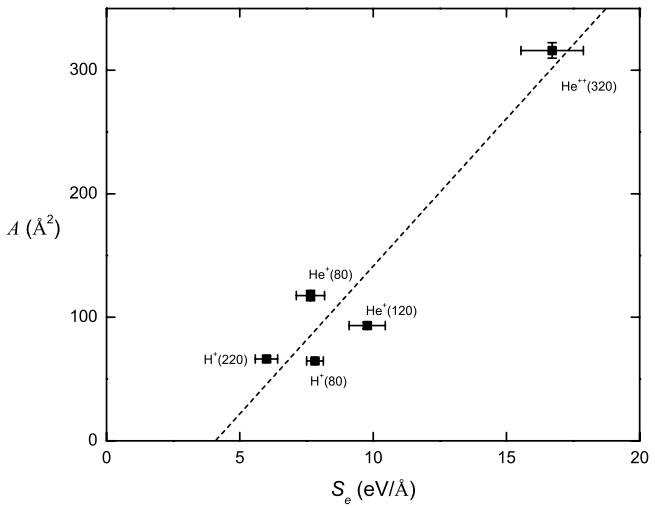

FIG. 3.—Compaction area A vs. electronic stopping power S_e for light ions. Each data point is labeled with the type of ion and its energy in keV. The horizontal bars give the dispersion between experimental measurements of S_e and SRIM values. The dashed line is a linear fit that suggests the existence of a threshold stopping power $S_t = 4$ eV Å^{-1}, below which no compaction occurs. The inverse of the slope is the effective energy density for compaction $\varepsilon = 0.04$ eV Å^{-3} = 1.3 eV molecule^{-1}.

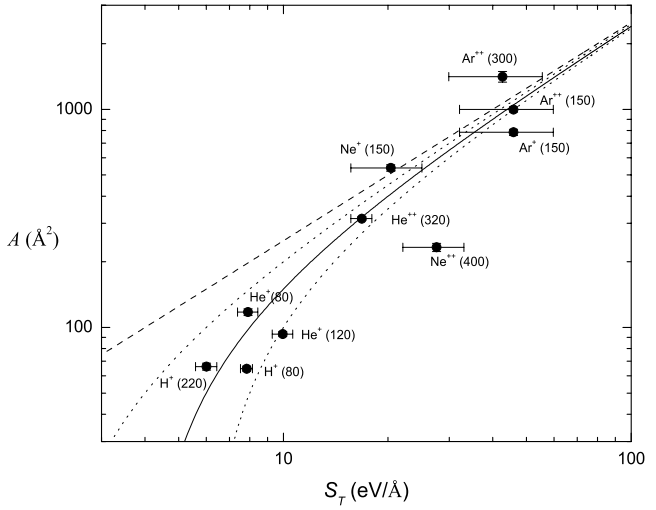

FIG. 4.—Compaction area A vs. total stopping power S_T for both light fast ions and slow heavy ions. Each data point is labeled with the type of ion and its energy in keV. The horizontal bars give the dispersion between experimental measurements of S_T and SRIM values. The solid line is fit of the form $A = (S_T - S_t)/\varepsilon$ for a threshold stopping value of 4 eV Å^{-1} and a effective energy density of 0.04 eV Å^{-3} as evaluated from Fig. 3. The dotted lines show how the fit degrades when the threshold S_t is changed by ± 2 eV Å^{-1}. The dashed line corresponds to $S_t = 0$.

R_m. In our energy range, where the maximum electron energy is a few hundred eV, R_m can be considered a constant with a typical value of $\sim$10 Å due to elastic scattering (Wolfgang 2001).

To test these models, we study the dependence of the compaction area A on S_e. We recall that A is obtained by fitting the measured fluence dependence of porosity (Fig. 2) to the expression $P(F) = P_0 \exp(-AF) + P_r$. In Figure 3, we show A vs. S_e for the light ions, which lose energy mainly through electronic processes. Since S_e changes during penetration as the ions slow down, we use a mean S_e, which we evaluate using SRIM (Ziegler & Biersack 2006). The stopping power in SRIM tables are fit to experimental data on water, which exist only for H (Bauer et al. 1994; Wenzel & Whaling 1952) and He (Matteson et al. 1977) projectiles. For Ne and Ar there are no experimental S_e data available for ice, and the values of SRIM are quite uncertain. We estimate the uncertainties, shown as horizontal bars in Figure 3, by comparing SRIM values with available experimental data for water and other targets (Fastrup et al. 1968; Hvelplund 1971; Weyl 1953).

Since the two models discussed above predict a linear dependence of the ion track area on the electronic stopping power, we fit the data in Figure 3 to a function $A = (S_e - S_t)/\varepsilon$. The fit gives $\varepsilon = 0.04$ eV Å^{-3} = 1.3 eV molecule^{-1} and $S_t = 4$ eV Å^{-1}. The factor ε can be interpreted as the effective density of deposited energy required to break hydrogen bonds and allow molecules to rearrange into compact ice. The value of ε is about twice the activation energy for self-diffusion, 0.6 eV (Lars & Runnels 1969). The existence of S_t, a threshold electronic stopping below which no compaction occurs ($A = 0$) is implied in the theories but not given explicitly. For $S < S_t$, it is likely that fluctuations of energy loss (straggling) will still produce some compaction of the ice film, but this condition would produce a discontinuous track, which would require a different theoretical treatment.

4.2. *Slow Heavy Ions*

We also irradiated porous ice films with slow heavy ions such as 150 keV Ne^+ and 150 keV Ar^{++}, as shown in Figure 2. These irradiations simulate the bombardment of the interstellar dust grains by keV stellar wind or interstellar shocks for which nuclear collisions are the dominant energy loss mechanism. The nuclear energy losses of the slow heavy ions chosen in our experiments is a significant fraction of the total energy loss, e.g., S_n is twice as large as S_e for 150 keV Ar. For these ions, the compaction data cannot be fitted by a linear dependence with S_e, suggesting that the energy deposited in nuclear processes should also contribute to compaction. In this case, "hot" regions in the sample can be created by elastic collisions between the projectiles and target nuclei and the cascade of recoils atoms. Although there are no analytical models that describe this complex case, we assume that the S_n dependence of the area of the compacted regions perpendicular to the ion path is also linear. As a first approximation, the nuclear and electronic energy losses act independently, which leads us to suggest an empirical relationship for the total compaction area of $A = (S_T - S_t)/\varepsilon$, where S_T is the sum of S_e and S_n. In Figure 4, we plot the total compaction area for both fast light ions and slow heavy ions vs. S_T. The solid line is a fit of the form $A = (S_T - S_t)/\varepsilon$, where S_t and ε are assigned the same values derived from experiments with fast light ions. As in Figure 3, the horizontal bars in Figure 4 represent the dispersion between the SRIM tables and available experimental values of the stopping power.

We propose that the threshold stopping and the effective energy density required to produce compaction is an intrinsic property of the solid, and does not depend on the mechanism by which the energy is delivered to the solid. To further emphasize the existence of the threshold, we also plot $A = (S_T - S_t)/\varepsilon$ for different values of S_t (dashed line showing $S_t = 0$ and dotted lines $S_t = 2$ eV Å^{-1} [*left*] and 6 eV Å^{-1} [*right*]).

4.3. *Dose Dependence*

A parameter typically used to compare results of different experiments is the radiation dose, the average energy absorbed per molecule. Since there is a threshold stopping power for compaction, we cannot use the dose as D (eV cm^{-3}) = FS_T, but instead must use the restricted stopping power $S_T - S_t$ (Turner 2007). In Figure 5, we plot the normalized porosity P_n of ice films irradiated with different ions at different energy as a function of the

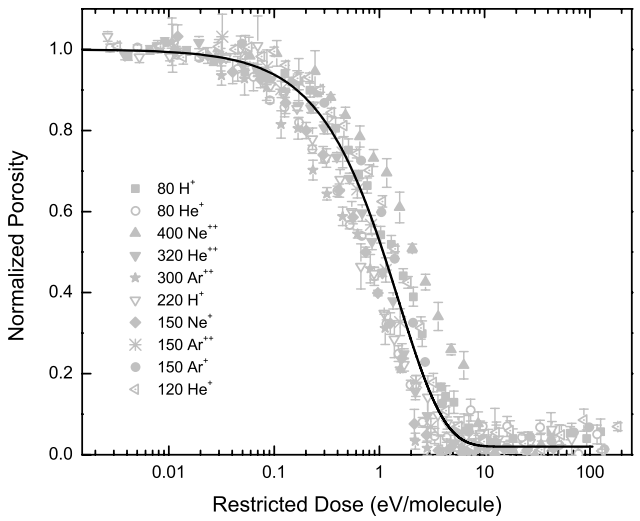

FIG. 5.—Dependence of normalized porosity on the restricted dose (eV molecule^{-1}) delivered to the ice (see text). The solid line is the averaged fit $\bar{P}_n(D_r) = \bar{P}_{n0}\exp(-D_r/\bar{D}_0) + \bar{P}_{nr}$, with $\bar{D}_0 = 1.52$ eV molecule^{-1}. [*See the electronic edition of the Journal for a color version of this figure.*]

restricted dose D_r (eV molecule^{-1}) $= F(S_T - S_t)/N$. We recall that F is the ion fluence and N is the ice density. The porosity is normalized to the average initial value.

Each data set shown in Figure 5 was fit with $P_n(D_r) = P_{n0}\exp(-D_r/D_0) + P_{nr}$, where P_{n0} and P_{nr} are the initial and the residual normalized porosities, and D_0 is the dose required to reduce the porosity by 63%. The solid line shown in Figure 5 is an average of the individual fits to all data sets. For the average, $\bar{D}_0 = 1.52$ eV molecule^{-1}. Since the spread of D_0 is within a factor of 2 around the mean, the average dose dependence may be used as a rough predictor for compaction by other ions.

5. ASTROPHYSICAL IMPLICATIONS

The compaction time τ for cosmic rays impacting interstellar ice with an energy flux $\Phi(E)$ is given by

$$\tau^{-1} = \sum_i \int A(E,i)\Phi_i(E)\,dE, \tag{3}$$

where i labels different cosmic ray species such as H or Fe, and $A(E, i)$ is the track area compacted by individual cosmic rays. From our experiments, $A(E,i) = [S_e(E,i) - S_t]/\varepsilon$. Thus,

$$\tau^{-1} = \frac{1}{\varepsilon}\left[\sum_i \int S_e(E,i)\Phi_i(E)\,dE - \sum_i \int S_t\Phi_i(E)\,dE\right]. \tag{4}$$

The fluxes $\Phi_i(E)$ cannot be measured directly, but have been estimated from measurements within the heliosphere. To reduce uncertainties in the estimation of τ, we relate it to an observable quantity, the ionization rate ζ of interstellar H_2 gas, which is also directly related to $\Phi_i(E)$ and the electronic stopping powers, this time on H_2, $S_e^*(E,i)$:

$$\zeta = \sum_i \int \frac{S_e^*(E,i)}{WN_{H_2}}\Phi_i(E)\,dE. \tag{5}$$

Here N_{H_2} is the hydrogen gas density, and W is the average energy required to produce an ionization, 37 eV for H_2 (ICRU 1979). We now introduce a scaling term $\alpha(E, i)$, to express ζ in terms of stopping power of the cosmic ray nuclei in water ice (which enters in eq. [3]), instead of hydrogen gas: $S_e^*/N_{H_2} = \alpha S_e/N_{ice}$, with $N_{ice} = 2.34\times10^{22}$ H_2O cm^{-3}. Thus,

$$\zeta = \sum_i \int \frac{\alpha(E,i)S_e(E,i)}{WN_{ice}}\Phi_i(E)\,dE. \tag{6}$$

The average value of the scaling term is $\bar{\alpha} \approx 0.4$ using stopping power values for H and Fe (Ziegler & Biersack 2006). The second term in equation (4), a small correction due to the threshold, can be estimated using analytical expressions for energy fluxes of Galactic cosmic rays (Bringa et al. 2007):

$$\Phi_H(E) = \frac{1.45E^{0.3}}{(E+0.12)^3},$$
$$\Phi_{Fe}(E) = \frac{0.22E^{0.3}}{(E+6.72)^3}, \tag{7}$$

where E is energy of the nuclei in GeV, and the particle fluxes Φ_i are given in (cm^2 s sr GeV)$^{-1}$. With these fluxes, we calculate that the threshold correction only amounts to 29% of the first term. Therefore, we can rewrite equation (4) as

$$\tau^{-1} = \frac{0.71N_{ice}}{\varepsilon}\sum_i \int \frac{S_e(E,i)}{N_{ice}}\Phi_i(E)\,dE. \tag{8}$$

Making the connection with equation (6) yields

$$\tau^{-1} = \frac{0.71N_{ice}W}{\varepsilon\bar{\alpha}}\sum_i \int \frac{S_e^*(E,i)}{WN_{H_2}}\Phi_i(E)\,dE. \tag{9}$$

Further simplification leads to

$$\tau^{-1} = \frac{0.71N_{ice}W}{\varepsilon\bar{\alpha}}\zeta. \tag{11}$$

Several studies (McCall et al. 1999; van der Tak & van Dishoeck 2000) have estimated the cosmic-ray ionization rate in the dense molecular clouds ζ to be $3 \pm 2\times10^{-17}$ s^{-1}. Thus, based on equation (11), porous ices on the dust grains will compact in $30\pm$ 20 million years. This lifetime is about an order of magnitude larger than a previous estimate (Palumbo 2006) based on the decrease in CO adsorption by ice irradiated by 200 keV protons and a model that approximates a cosmic-ray flux as 1 MeV proton cm^{-2} s^{-1}. Our compaction time is 2 orders of magnitude larger than the accretion time of ice mantles in dense clouds (Tielens & Allamandola 1987) and comparable to or smaller than the estimated grain lifetimes of 30–500 million years (Greenberg 1982).

Finally, we note that, although the total H nuclei flux is $\sim10^4$ times larger than the Fe flux, the Fe CRs dominate compaction due to their higher stopping power. Only 10 to 400 keV protons contribute to interstellar ice compaction, because they are the ones with $S_e > S_t$. In contrast, all Fe nuclei in the relevant energy range (10^{-3} to 10 GeV) contribute to ice compaction, since they all have $S_e > S_t$.

This paper is based on work supported by the National Science Foundation under grant AST0506565.

REFERENCES

Bauer, P., Käferböck, W., & Necas, V. 1994, Nucl. Instrum. Methods Phys. Res. B, 93, 132
Bringa, E. M., et al. 2007, ApJ, 662, 372
Fastrup, B., Borup, A., & Hvelplund, P. 1968, Canadian J. Phys., 46, 489
Greenberg, J. M. 1982, in IAU Colloq. 61, Comets: Discoveries, Statistics, and Observational Selection (Tucson: Univ. Arizona Press), 131
Horimoto, N., Kato, H. S., & Kawai, M. 2002, J. Chem. Phys., 116, 4375
Hvelplund, P. 1971, Kgl. Danske Videnskab. Selskab, Mat.-Fys. Medd., 38
ICRU. 1979, ICRU Rept. 31
Keane, J. V., Tielens, A., Boogert, A. C. A., Schutte, W. A., & Whittet, D. C. B. 2001, A&A, 376, 254
Kimmel, G. A., Stevenson, K. P., Dohnalek, Z., Smith, R. S., & Kay, B. D. 2001, J. Chem. Phys., 114, 5284
Lars, O., & Runnels, L. K. 1969, J. Chem. Phys., 50, 1089
Matteson, S., Powers, D., & Chau, E. K. L. 1977, Phys. Rev. A, 15, 856
Mayer, E., & Pletzer, R. 1986, Nature, 319, 298
McCall, B. J., Geballe, T. R., Hinkle, K. H., & Oka, T. 1999, ApJ, 522, 338
Narten, A. H., Venkatesh, C. G., & Rice, S. A. 1976, J. Chem. Phys., 64, 1106
Palumbo, M. E. 2006, A&A, 453, 903
Raut, U., Fama, M., Teolis, B. D., & Baragiola, R. A. 2007a, J. Chem. Phys., 127, 204713
Raut, U., Teolis, B. D., Loeffler, M. J., Vidal, R. A., Fama, M., & Baragiola, R. A. 2007b, J. Chem. Phys., 126, 244511
Rowland, B., & Devlin, J. P. 1991, J. Chem. Phys., 94, 812
Stevenson, K. P., Kimmel, G. A., Dohnalek, Z., Smith, R. S., & Kay, B. D. 1999, Science, 283, 1505
Szenes, G. 1992, Mat. Sci. Forum, 97–99, 647
———. 1995, Phys. Rev. B, 51, 8026
———. 1997, Nucl. Instrum. Methods Phys. Res. B, 122, 530
Tielens, A. G. G. M., & Allamandola, L. J. 1987, in Physical processes in interstellar clouds
Turner, J. E. 2007, Atoms, Radiation, and Radiation Protection (3rd ed.; Berlin: Wiley)
van der Tak, F. F. S., & van Dishoeck, E. F. 2000, A&A, 358, L79
Waligorski, M. P. R., Hamm, R. N., & Katz, R. 1986, Nucl. Tracks Radiat. Meas., 11, 309
Watson, C. C., & Tombrello, T. A. 1985, Radiat. Effects and Defects in Solids, 89, 263
Wenzel, W. A., & Whaling, W. 1952, Phys. Rev., 87, 499
Weyl, P. K. 1953, Phys. Rev., 91, 289
Wolfgang, S. M. W. 2001, Surface and Interface Analysis, 31, 141
Ziegler, J. F., & Biersack, J. P. 2006, SRIM: The Stopping and Range of Ions in Matter, http://www.srim.org/#SRIM